Hard Magnetic Materials

Toward Realization of Bulk $L1_0$-FeNi

Dimitrios Niarchos[1,2], Margarit Gjoka[1], Vassilis Psycharis[1], Alexandra Ioannidou[1], Eamonn Devlin[1], Athanasios Sigalos[2], and Dimitrios I. Anyfantis[2]

[1]*Institute of Nanoscience and Nanotechnology, NCSR Demokritos, 15341 Paraskevi, Greece*
[2]*AMEN New Technologies, 15343 Paraskevi, Greece*

Received 16 Dec 2025, revised 3 Feb 2026, accepted 7 Feb 2026, published 11 Feb 2026, current version 18 Mar 2026.

Abstract—In this letter, we demonstrate for the first time the preparation of bulk $L1_0$-FeNi embedded in an fcc FeNi by alloying Fe and Ni during casting with 5%–10% indium metal and annealing at 350 °C for a week. From X-ray diffraction, magnetization, and Mössbauer data, we have strong indications that the $L1_0$-FeNi phase is formed and coexists with the cubic A1-FeNi at a ratio of 30/70 for the sample with 5% In and 20/80% for the sample with 10% In, as derived from X-ray diffraction. This finding is supported by the Mössbauer data, where the ratio of $L1_0$-FeNi to A1-FeNi is 48/52 and 24/76, respectively. The morphology of the alloys is sponge-like and very brittle, and the final In stoichiometry is much less than the nominal one.

Index Terms—Hard magnetic materials, $L1_0$-FeNi bulk, permanent magnets.

I. INTRODUCTION

Electrification of drive systems is an ongoing trend in all kinds of transportation applications. Whereas line-based systems, such as electric trains and electric buses, are long-time well established, new applications are continuously emerging, ranging from e-scooters to e-bikes to e-cars and e-trucks. Even e-planes have been demonstrated. They all benefit from the eco-friendliness of the electric propulsion system, its zero emissions, zero noise, high torque, and high efficiency. Permanent-magnet-excited synchronous electric motors are among the most efficient electrical machines due to their high density (torque/weight) and efficiency (mileage/kWh).

Among all available permanent magnets, Nd–Fe–B magnets with a small addition of Dy are the most powerful magnets in the temperature range up to 200 °C with a high remanence and a high coercivity ($Hc > 500$ kA/m) and an energy product of the order of 420–450 kJ/m^3 [Gutfleish 2011, Wang 2016, Coey 2020]. The Dy-containing Nd-Fe-B magnets are far more expensive than other lower grade rare-Earth-less types of magnets (gap magnets) [Ormerod 2019] but still affordable enough to be widely used in industry. A second class of important permanent magnets is of the type sintered $SmCo_5$ and $Sm_2(Co,Fe,Cu,Zr)_{17}$ magnets, which were developed in the late 1960s and 1970s, respectively. The $SmCo_5$ magnet has very high magnetocrystalline anisotropy, which results in high intrinsic coercivity. The maximum energy product of $SmCo_5$ magnets is ∼144–160 kJ/m^3 [Kumar 1988]. A shortage of Co in the 1970's led the scientists to replace Co with Fe and to develop coercivity. Cu and Zr were introduced to $Sm_2(Co,Fe)_{17}$, which has a maximum energy product as high as 260 kJ/m^3 [Guo 2006].

Because of supply risk and increasing demand, Nd and Dy are considered to be critical elements [European Commission 2023]. In order to cope with the supply risk, magnet producers and users aim for rare-Earth-lean or rare-Earth-free permanent magnets. With respect to the magnet's performance, rare-Earth lean or rare-Earth-free permanent magnets may fill a gap between ferrites and NdFeB magnets [Ormerod 2019]. Several new candidate materials systems were investigated, and some have shown realistic potential for replacing RE PMs for various applications. These materials systems include Mn-based high magnetocrystalline anisotropy alloys (MnBi and MnAl–C compounds) [Cui 2018], iron-based nitride/carbide systems, such as the high saturation magnetization $Fe_{16}N_2$-type phase [Wang 2020] and the high coercivity tetrataenite $L1_0$ phase of FeNi and FeCo.

Among these, the best candidates for rare-Earth-free magnets, the $L1_0$-FeNi alloy, are very attractive because they have a large uniaxial magnetic anisotropy energy with Ku $\sim 1.3 \times 10^6$ J/m^3, nearly the same saturation magnetization, $\mu_0 M_s = 1.59$ T, as $Nd_2Fe_{14}B$, a high Curie temperature (>550 °C), and a theoretically possible energy product $(BH)_{max} = 448$ kJ/m^3 [Kovacs 2017, Fischbacher 2018]. The $L1_0$-type structure was first produced by Néel [1964] and Pauleve [1968] with a stoichiometry of $Fe_{50}Ni_{50}$ by the creation of vacancies–dislocations with neutron irradiation, yielding an estimated order–disorder transformation temperature around 320 °C, which is very low compared to the other $L1_0$ alloys. This low temperature results in slow diffusion of the Fe and Ni atoms, making the transformation extremely sluggish. The only bulk $L1_0$-FeNi sample has been found in meteorites, where it took billions of years to transform [Poirier 2015]. Recent efforts have succeeded in the preparation of $L1_0$-FeNi in thin films on special substrates, which promote the tetragonal structure [Kojima 2011]. However, to be considered for applications, bulk tetragonal $L1_0$-FeNi samples must be prepared. The high stability of the crystalline phase, together with the low diffusivity around the transformation temperature, makes the formation of bulk $L1_0$-FeNi extremely difficult. Approaches to increase the diffusivity of Fe and Ni by nonequilibrium processes include energy electron irradiation [Chamberod 1979], melt-spinning [Sato 2016], and severe plastic deformation [Lee 2014]. The key behind these approaches is to create vacancies, thus enhancing the diffusivity, leading to faster atomic migration and partial ordering. The most successful attempt to prepare bulk $L1_0$-FeNi is by Makino [2015], employing a new route based on

Corresponding author: Dimitris Niarchos (e-mail: d.niarchos@inn.demokritos.gr).
Digital Object Identifier 10.1109/LMAG.2026.3663904

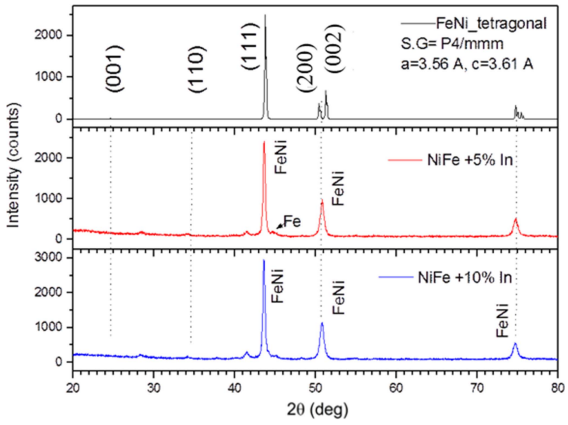

Fig. 1. XRD of FeNi-x(In), $x = 5$ and 10%, together with (top panel) the simulated $L1_0$ structure using $a = 3.56$ Å and $c = 3.61$ Å [Makino 2015].

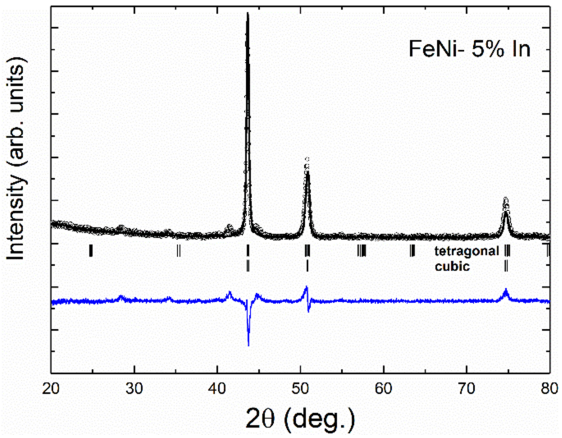

Fig. 2. Rietveld analysis of the FeNi −5% In sample. Data are given in Table 1.

the fact that the diffusivity of atoms is faster in amorphous alloys during crystallization. By selecting a low-temperature (<400 °C) crystallization alloy of the type $Fe_{42}Ni_{41.3}Si_xB_{12-x}P_4Cu_{0.7}$ ($x = 2$ to 8%), they succeeded in precipitating a small fraction of the $L1_0$-FeNi into the amorphous matrix. Although attempts to stabilize the $L1_0$-FeNi were most successful in thin films or in amorphous materials, the chemical ordering is much smaller in most other attempts to fabricate $L1_0$-FeNi. Goto [2017] synthesized $L1_0$-FeNi powder with a degree of order of 0.7 through nitrogen insertion and topotactic extraction, achieving a coercivity of 0.18 T. Textured $L1_0$-FeNi films [Ito 2019] were fabricated by denitriding FeNiN films on epitaxially grown (001) substrates, yielding a Ku value of about 0.44×10^6 J/m^3 with a degree of order of 0.4. Very recently, a study [Ivanof 2022] reported the successful alloy casting of $L1_0$-FeNi by adding phosphorus and carbon, which accelerates the diffusion and the formation of the tetragonal ordered structure. On the other hand, first-principles calculations [Tuvshin 2021] revealed that a B-doped $L1_0$-FeNi phase could exhibit improved structural stability and enhanced intrinsic magnetic properties, such as Ku values up to 2.6 MJ m^{-3}. Mandal [2023] investigated the formation of $L1_0$-FeNi via mechanical alloying followed by field-assisted heat treatment to increase the ordering parameter, phase content, and magnetic properties. A recent study [Lewis 2023] further demonstrated that controlled thermal processing can induce partial atomic ordering in bulk FeNi alloys, forming tetrataenite with measurable magnetocrystalline anisotropy and highlighting the material's potential as a sustainable candidate for next-generation permanent magnets.

In this work, we have employed a different approach. At low stoichiometries, In does not alloy with either Fe or Ni. We cast FeNi with In (melting point 156.6 °C), making a solid solution of FeNi–In. Following this approach, we managed to produce a very large percentage of $L1_0$-FeNi in a cubic matrix of FeNi, as confirmed by the techniques used in this study, such as X-ray diffraction (**XRD**), magnetization, Mössbauer, and element profile analysis using a Phenom Pro scanning electron microscopy (**SEM**).

II. EXPERIMENTAL DETAILS

Samples of approximately 4 g were prepared by radio frequency induction melting together in a Cu cold crucible and an Ar atmosphere of high-purity Fe, Ni, and In metals at a stoichiometry of $Fe_{50}Ni_{50}$ with an addition of 5 and 10% wt. In acting as a flux. The samples were annealed at 350 °C for 72 h according to literature reports to promote $L1_0$ ordering while minimizing grain growth [Lewis 2023]. The ingots were remelted three times, observing each time In vapor condensing on the quartz tube. The final ingot was very brittle, with a sponge-like texture that was easily pulverized. In contrast, ingots containing the same addition of Ag were very hard to pulverize and remained fcc. XRD data were collected on a D500 Siemens diffractometer using copper Kα radiation, and the fitting was done using Rietveld software. Magnetization data were collected using a vibrating sample magnetometer (PAR155) and a superconducting quantum interference device (**SQUID**) (Quantum Design) magnetometer. The Curie temperature was measured with the Pyris (PerkinElmer) thermogravimetric system in thermomagnetic mode. Mössbauer data were collected with a constant acceleration system using a ^{57}Co(Rh) source activity (50 mCi, at the time of measurement), and SEM data were collected with a tabletop PHENON PRO system equipped with energy-dispersive X-ray (**EDAX**) analysis.

III. RESULTS

A. Crystallographic Data

In Fig. 1, the XRD data of the alloys with 5% In and 10% In are shown together with the theoretical fit using crystallographic data from literature.

The structures for the as-cast alloys are similar, with some minor impurities and, significantly, an absence of the superlattice reflection lines (001) and (110). An additional characteristic of the tetragonal $L1_0$-FeNi structure is the splitting of the (200) reflection into the (200) and (002) peaks at ∼51°, which appears as a broadened line in our samples due to the coexistence of fcc FeNi and $L1_0$-FeNi phases. Other factors, such as nanocrystallinity and microstrains, can also enhance this effect. The missing superlattice reflections (001) and (110) of the $L1_0$-ordered structure are related to the difference of the scattering factors $|f_{Fe} - f_{Ni}|^2$; as these are very similar for Fe and Ni, the intensity is extremely weak, and they can only be observed with synchrotron diffraction [Cui 2018, Wang 2020]. Furthermore, as the a and c lattice constants are very close in value, we can conclude that we do not have a complete ordering of our sample. In order to see if the $L1_0$ phase is formed, we proceeded with a Rietveld analysis of the two samples, and the results are given in Table 1 and Fig. 2.

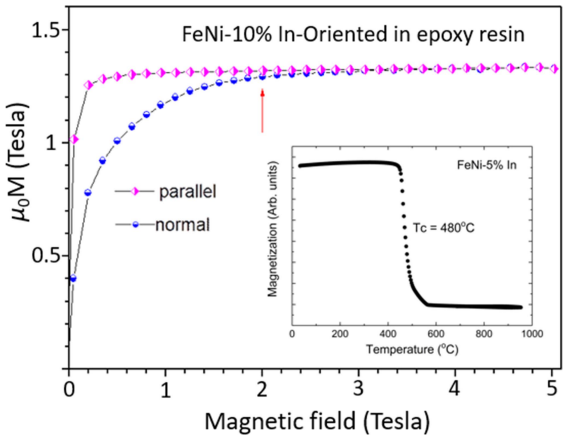

Fig. 3. Anisotropy field values in samples oriented in epoxy in an applied field of 2 T. The inset shows the Curie temperature of the FeNi-x(In) sample with $x = 5\%$. The values are within the range of expected tetragonal phases, which vary from 450 °C to 550 °C.

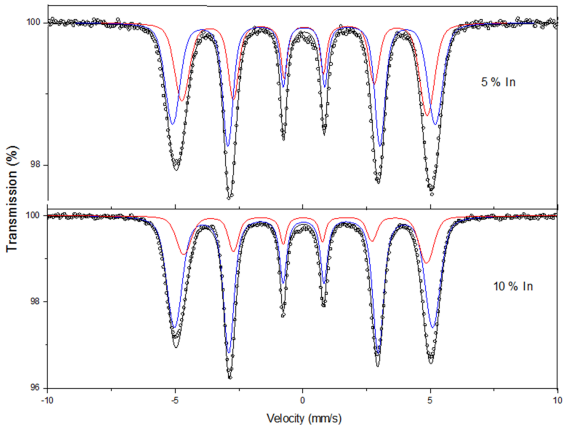

Fig. 4 Mössbauer spectra of (top) FeNi-5% In and (bottom) FeNi-10% In. The measured data are shown by the black dots, and the fitting lines are shown by the black lines on the measured data. The component from the A1 phase (blue lines) and that from the $L1_0$ phase (red lines) are also shown for each spectrum, shifted below the measured data.

Table 1. Crystallographic data after Rietveld.

In content	Phase	Phase content (%)	a (Å)	c (Å)
5%	$L1_0$	30	3.583(1)	3.606(1)
	A1	70	3.594(1)	-
10%	$L1_0$	20	3.590(1)	3.616(1)
	A1	80	3.599(1)	-

Space Group: $L1_0$: P4/mmm, A1:Fm-3m.

To estimate the degree of order, quantitative analysis of integrated intensities of the XRD pattern is a commonly used technique. However, in this study, it is difficult to employ this technique, due to the extremely weak intensity of superlattice reflections and a c-axis orientation texture. Coexistence of disordered FeNi, ordered FeNi, and Ni-rich fcc FeNi phases also makes the intensity analysis difficult for oriented samples. We are planning to do diffraction experiments at the synchrotron measurements to elucidate this issue.

Table 2. Mössbauer parameters for the 5% and 10% In samples, together with published data for comparison.

Sample/Phase	QS ($eQV_{zz}/2$, mm/s)	Hyperfine field (kOe)	Area %
FeNi-5% In			
$L1_0$	0.43	297	42
A1	0.00	320	58
FeNi-10% In			
$L1_0$	0.52	294	24
A1	0.00	315	76
FeNi	0.63	295–312	<43
[Mibu 2015]	0.00	320–330	>57

B. Magnetization Data

The Curie temperatures of both samples are the same, $T_c \sim 480$ °C, and are consistent with the published literature values, which vary from 450 °C–550 °C [Guo 2006, Wang 2016]. A characteristic of these data is the absence of α-Fe, consistent with the XRD data [Fischbacher 2018]. Magnetization data were obtained with a SQUID magnetometer in a maximum field of 5 T at room temperature (**RT**) in an epoxy-oriented sample. Curie temperatures were obtained using a Pyris thermogravimetric system, as shown in Fig. 3 for the 5% In sample (the same result applies to the 10% In sample).

An anisotropy field, consistent with a tetragonal structure, of approximately 2 T, was obtained from measurements on epoxy-oriented powders, as shown in Fig. 3, corrected for demagnetizing fields, and it is very close to the expected theoretical value, considering an anisotropy constant Ku $\sim 1.3 \times 10^6$ J/m^3 and a saturation magnetization $\mu_0 M_s = 1.38$ T.

C. Mössbauer Data

The ^{57}Fe Mössbauer spectra were obtained at 300 K on a conventional constant acceleration spectrometer with a ^{57}Co(Rh) source moving at RT and calibrated with α-Fe foil at RT. The spectra can be fitted with two magnetic sites, as shown in Fig. 4. In Table 2, we list the fitting parameters used.

In agreement with XRD data, Mössbauer results indicate that our spectra consist of one magnetic site with almost zero quadrupole splitting (**QS**) and a hyperfine field of ~32 T indicative of the cubic FeNi phase (A1) and a second site with a hyperfine field ~29 T and large QS values, 0.43 and 0.52 mm/s for the 5% and 10% In samples, respectively, which can be assigned to a tetragonal $L1_0$-FeNi phase [Mibu 2015]. These values are larger than the values measured in meteorites [Larsen 1982], indicative of a less perfectly ordered $L1_0$ structure. The difference between the $L1_0$ phase fractions obtained from XRD and Mössbauer spectroscopy arises from their distinct sensitivities: XRD probes long-range crystallographic order, whereas Mössbauer spectroscopy reflects the local chemical environment of Fe atoms, which may remain partially disordered within crystallographically tetragonal regions.

D. EDAX and Microstructure Data

In an attempt to elucidate the role of In during and after annealing, we have performed an element-selective EDAX analysis, and the results are shown in Fig. 5. The granular morphology of the alloy shows grain sizes varying from a few micrometers up to tens of micrometers.

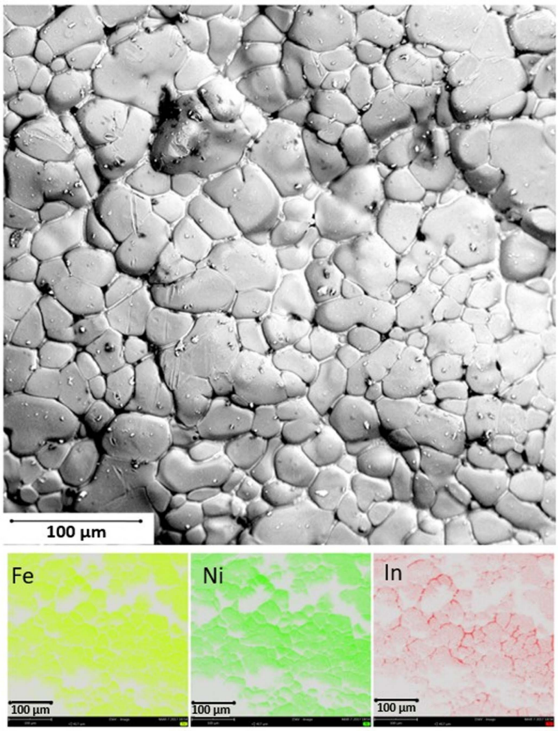

Fig. 5. Morphology and selective element analysis using EDAX for the 5% In (nominal) concentration.

Although the Fe/Ni ratio is close to 50%, the average In content is approximately half of the nominal composition, as it was derived from EDAX analysis. Element-specific analysis for Fe, Ni, and In shows a uniform distribution of FeNi grains that are surrounded by In. The final alloy composition was estimated as $Fe_{50}Ni_{50}$ with ~2.5 wt% In. This may be expected due to the fact that In has a much lower melting point compared to Fe and Ni, and during cooling, first, the FeNi is formed, and then In solidifies, coating each grain, without any indication of a bulk alloy of the type FeNi–In. In addition, In promotes $L1_0$ phase formation due to its substantially lower surface energy relative to Fe and Ni, leading to preferential surface segregation and a reduction in the overall surface free energy of the FeNi system. Moreover, its larger atomic radius, very limited solid solubility in FeNi, and weak chemical affinity with the FeNi bulk further disfavor incorporation into the lattice.

IV. DISCUSSION

In Fig. 6, the arrangement of the atoms in the unit cell is shown in order to distinguish the two crystallographic structures of the FeNi, namely, the $L1_0$-ordered phase [Fig. 6(a)] and the disordered A1 phase (disordered cubic fcc). From the unit cells in Fig. 6, it is expected from XRD data that we can distinguish the tetragonal from the cubic phase, which indeed is the case. The full tetragonal $L1_0$-FeNi phase has lattice parameters $a = 3.5761$–3.582 Å and $c = 3.589$–3.607 Å [Wang 2016], and the cubic A1 structure is $a = c = 3.602$ Å. Our XRD values derived from the Rietveld analysis fall in this range and confirm that two phases coexist with a ratio varying with a percentage of In. Both samples have Curie temperatures around 480 °C, a value between the fcc FeNi of 250 °C and the value of the full $L1_0$-FeNi, which is higher than 550 °C

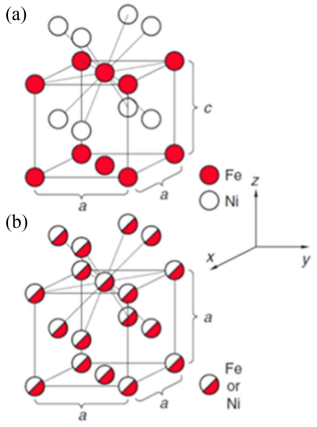

Fig. 6. (a) $L1_0$-FeNi ordered phase and (b) A1-fcc disordered phase of FeNi. Notice, that in the $L1_0$-phase, there are two crystallographically inequivalent sites, one with cubic symmetry and the other with tetragonal symmetry, although in the A1-phase, all iron sites have cubic symmetry [Mibu 2015].

[Fischbacher 2018]. Such a value is consistent also with our XRD data and anisotropy measurements that we have obtained for a not fully ordered $L1_0$-FeNi. The cubic phase has a zero-anisotropy field, so the value of approximately 2 T can be assigned only to the hard tetragonal phase, which is also consistent with saturation magnetization data of our sample of $\mu_0 M_s = 1.38$ T and a theoretical anisotropy Ku ~1.3×10^6 J/m^3. In addition, supportive data that our approach leads to the formation of the $L1_0$-FeNi phase come from Mössbauer data, where we unambiguously do have two subspectra, one with cubic symmetry and the other with tetragonal symmetry. The hyperfine field values are consistent with the study on thin films [Kovacs 2017], where the largest hyperfine field is assigned to the A1 phase, close to the a-Fe (33 T), and the smallest one, with an average value of 29.5 T, to the tetragonal one. However, the critical parameter, which distinguishes the two coexisting phases, is the QS, which is zero for Fe in a cubic environment (A1) and has a relatively large value for Fe in a tetragonal environment, as it is the case for the $L1_0$-phase. Other factors, such as nanocrystallinity and microstrains, can also enhance this effect. No traces of a-Fe were detected, consistent with the thermomagnetic data.

Previous efforts to prepare bulk $L1_0$-FeNi alloys were based on the acceleration of diffusion of Fe and Ni by the creation of vacancies or dislocations, and more recently [Ormerod 2019] by the acceleration of the diffusion of atoms when they are embedded in an amorphous matrix. Regarding the mechanism of the formation of the $L1_0$-FeNi by the addition of In during casting, we have no concrete idea. We suspect, that at the initial stage of casting, a solid solution of FeNi–In is formed, and then as we are heating to homogenize the alloy, the low-melting In separates and partially evaporates, leaving behind some vacancies where Fe and Ni diffuse and stabilize the tetragonal phase. A solid solution can be considered as an "amorphous-like" state, as the one formed by Cui [2018], which leads to the acceleration of the Fe and Ni diffusion; this remains a phenomenological hypothesis requiring detailed theoretical or experimental verification in future work. Alternatively, In acts as a flux, allowing the Fe and Ni atoms to diffuse faster and, under the proper thermal conditions, to form one phase or the other. Whatever the mechanism is, which we will unravel by making more samples and collecting more data from additional techniques, we

have strong evidence of bulk $L1_0$-FeNi formation, which can lead to novel permanent magnets without rare-Earth elements.

V. CONCLUSION

In this letter, we have demonstrated that bulk $L1_0$ can be obtained by direct casting of Fe and Ni in the presence of low In additions (∼5 wt%). Although crystallographically we cannot distinguish the superlattice peaks of $L1_0$, our magnetization data, the Curie temperature, and especially Mössbauer data clearly indicate that in our samples, there is a coexistence of fcc FeNi with $L1_0$-FeNi with a significant degree of ordering. Importantly, identification of the $L1_0$ phase in our work does not rely solely on XRD, but on converging evidence from the broadening of the (002) and (020) in Fig. 1, the lattice parameters derived from Rietveld refinement, finite magnetic anisotropy fields, the Curie temperatures, and more importantly, from the nonzero QS in Mössbauer spectra, which directly indicate tetragonal symmetry at the Fe site. While the exact microscopic role of In cannot be resolved within the scope of this study, the enhancement of ordering is consistent with vacancy-assisted and transient flux-assisted diffusion mechanisms. The sponge-like and brittle microstructure reflects the current processing route and is not application-ready; future work will address densification, microstructural control, and mechanical optimization. Nevertheless, these results establish a new pathway for fabricating bulk ordered FeNi, supporting its potential as a rare-Earth-free permanent magnet.

REFERENCES

Chamberod A, Laugier J, Penisson J M (1979), "Electron irradiation effects on iron-nickel invar alloys," *J. Magn. Magn. Mater.*, vol. 10, Art. no. 139, doi: 10.1016/0304-8853(79)90165-3.

Coey J M D (2020), "Perspective and prospects for rare Earth permanent magnets," *Engineering*, vol. 6, pp. 119–131, doi: 10.1016/j.eng.2018.11.034.

Cui J, Kramer M, Zhou L, Liu F, Gabay A, Hadjipanayis G, Balasubramanian B, Sellmyer D (2018), "Current progress and future challenges in rare-Earth-free permanent magnets," *Acta Materialia*, vol. 158, pp. 118–137, doi: 10.1016/j.actamat.2018.07.049.

European Commission (2023), "Critical raw materials, internal market, industry," Entrepreneurship and SMEs. [Online]. Available: https://ec.europa.eu/growth/sectors/raw-materials/specific-interest/critical_en

Fischbacher J, Kovacs A, Gusenbauer M, Oezelt H, Exl L, Bance S, Schrefl T (2018), "Micromagnetics of rare-Earth efficient permanent magnets," *J. Phys. D: Appl. Phys.*, vol. 51, Art. no. 193002, doi: 10.1088/1361-6463/aab7d1.

Goto S, Kura H, Watanabe E, Hayashi Y, Yanagihara H, Shimada Y, Mizuguchi M, Takanashi K, Kita E (2017), "Synthesis of single-phase $L1_0$-FeNi magnet powder by nitrogen insertion and topotactic extraction," *Sci. Rep.*, vol. 7, Art. no. 13216, doi: 10.1038/s41598-017-13562-2.

Guo &Zgr; &EEgr;, Pan W, Li W (2006), "Sm(Co,Fe,Cu,Zr)z sintered magnets with a maximum operating temperature of 500 °C," *J. Magn. Magn. Mater.*, vol. 303, pp. e396–e401, doi: 10.1016/j.jmmm.2006.01.107.

Gutfleisch O, Willard M A, Brück E, Chen C H, Sankar S G, Liu J P, (2011), "Magnetic materials and devices for the 21st century: Stronger, lighter, and more energy efficient," *Adv. Mater.*, vol. 23, pp. 821–842, doi: 10.1002/adma.201002180.

Ito K, Hayashida M, Mizuguchi M, Suemasu T, Yanagihara H, Takanashi K (2019), "Fabrication of $L1_0$-FeNi films by denitriding FeNiN films," *J. Magn. Soc. Jpn.*, vol. 43, pp. 79–83, doi: 10.3379/msjmag.1907R002.

Ivanof Y, Sarac B, Ketov S., Eckert J, Greer A L (2022), "Direct formation of hard-magnetic tetrataenite in bulk," *Adv. Sci.*, vol. 10, Art. no. 2204315, doi: 10.1002/advs.202204315.

Kojima T, Mizuguchi M, Koganezawa T, Osaka K, Kotsugi M, Takanashi K (2011), "Magnetic anisotropy and chemical order of artificially synthesized $L1_0$-ordered FeNi films on Au-Cu-Ni buffer layers," *Jpn. J. Appl. Phys.*, vol. 51, Art. no. 064207, doi: 10.1143/JJAP.51.010204.

Kovacs A, Fischbacher J, Oezelt H, Schrefl T, Kaidatzis A, Salikhov R, Farle M, Giannopoulos G, Niarchos D (2017), "Micromagnetic simulations for coercivity improvement through nano-structuring of rare-Earth-free $L1_0$-FeNi magnets," *IEEE Trans. Magn.*, vol. 53, Art. no. 7002205, doi: 10.1109/TMAG.2017.2701418.

Kumar K (1988), "$RETM_5$ and RE_2TM_{17} permanent magnets development," *J. Appl. Phys.*, vol. 63, pp. R13–R57, doi: 10.1063/1.341084.

Larsen L, Roy-Poulsen H, Roy-Poulsen N.O., Vistisen L, Knudsen J.M. (1982), "Order-disorder transitions in iron-nickel (50%-50%) alloys from iron meteorites as studied by mössbauer spectroscopy," *Phys. Rev. Lett.*, vol. 48, Art. no. 1054, doi: 10.1103/PhysRevLett.48.1054.

Lee S, Edalati K, Iwaoka H, Horita Z, Ohtsuki T, Ohkochi T, Kotsugi M, Kojima T, Mizuguchi M, Takanashi K (2014), "Formation of FeNi with $L1_0$-ordered structure using high-pressure torsion," *Philos. Mag. Lett.*, vol. 94, pp. 639–646, doi: 10.1080/09500839.2014.955546.

Lewis L H, Stamenov P S (2023), "Accelerating nature: Induced atomic order in equiatomic FeNi," *Adv. Sci.*, vol. 11, Art. no. 2302696, doi: 10.1002/advs.202302696.

Makino A, Sharma P, Sato K, Takeuchi A, Zang Y, Takenara K (2015), "Artificially produced rare-Earth free cosmic magnet," *Sci. Rep.*, vol. 5, Art. no. 16627, doi: 10.1038/srep16627.

Mandal S, Panigrahi A, Rath A, Bönisch M, Sengupta P, Debata M, Basu S (2023), "Formation of $L1_0$ ordering in FeNi by mechanical alloying and field-assisted heat treatment: Synchrotron XRD Studies," *ACS Omega*, vol. 8, pp. 13690–13701, doi: 10.1021/acsomega.2c07869.

Mibu K, Kojima T, Mizuguchi M, Takanashi K (2015), "Local structure and magnetism of $L1_0$-type FeNi alloy films with perpendicular magnetic anisotropy studied through 57Fe nuclear probes," *J. Phys. D: Appl. Phys.*, vol. 48, Art. no. 205002, doi: 10.1088/0022-3727/48/20/205002.

Néel L M, Pauleve J, Pauthenet R, Laugier J, Dautreppe D (1964), "Magnetic properties of an iron-nickel single crystal ordered by neutron bombardment," *J. Appl. Phys.*, vol. 35, pp. 873–876, doi: 10.1063/1.1713516.

Ormerod J (2019), "Rare Earth magnets: Yesterday, today and tomorrow," Magnetics, January 23-24, FL. [Online]. Available: https://www.slideshare.net/JohnOrmerod/2019-01-17-magnetics-2019

Pauleve J, Chamberod A, Krebs K, Bourret A (1968), "Magnetization curves of FeNi (50-50) single crystals ordered by neutron irradiation with an applied magnetic field," *J. Appl. Phys.*, vol. 39, pp. 989–990, doi: 10.1063/1.1656361.

Poirier E, Pinkerton F E, Kubic R, Mishra R K, Bordeaux N, Mubarok A, Lewis L H, Goldstein J I, Skomski R, Barmak K (2015), "Intrinsic magnetic properties of $L1_0$ FeNi obtained from meteorite, NWA 6259," *J. Appl. Phys.*, vol. 117, Art. no. 17E318, doi: 10.1063/1.4916190.

Sato K, Sharma P, Zhang Y, Takenaka K, Makino A (2016), "Crystallization induced ordering of hard magnetic $L1_0$ phase in melt-spun FeNi-based ribbons," *AIP Adv.*, vol. 6, Art. no. 055218, doi: 10.1063/1.4952968.

Tuvshin D, Ochirkhuyag T, Hong S C, Odkhuu D (2021), "First-principles prediction of rare-Earth free permanent magnet: FeNi with enhanced magnetic anisotropy and stability through interstitial boron," *AIP Adv.*, vol. 11, Art. no. 015138, doi: 10.1063/9.0000127.

Wang J P (2020), "Environment-friendly bulk $Fe_{16}N_2$ permanent magnet: Review and prospective," *J. Magn. Magn. Mater.*, vol. 497, Art. no. 165962, doi: 10.1016/j.jmmm.2019.165962.

Wang Z, Ju J, Wang J, Yin W, Chen R, Li M, Jin C, Tang X, Lee D, Yan A, (2016), "Magnetic properties improvement of die-upset Nd-Fe-B magnets by Dy-Cu press injection and subsequent heat treatment," *Sci. Rep.*, vol. 6, Art. no. 38335, doi: 10.1038/srep38335.

The Open Access publication of this article was financially supported by HEAL-Link.